Astron. Astrophys. 142, 71–84 (1985)

ASTRONOMY AND ASTROPHYSICS

The quasars 1038+528 A and B

J. M. Marcaide[1,2], I. I. Shapiro[1,3], B. E. Corey[1,4], W. D. Cotton[5], M. V. Gorenstein[1,3], A. E. E. Rogers[4], J. D. Romney[2], R. E. Schild[3], L. Bååth[6], N. Bartel[1,3], N. L. Cohen[1,3,7], T. A. Clark[8], R. A. Preston[9], M. I. Ratner[1,3], and A. R. Whitney[4]

[1] Massachusetts Institute of Technology, 77 Massachusetts Ave., Cambridge, MA 02139, USA
[2] Max-Planck-Institut für Radioastronomie, Auf dem Hügel 69, D-5300, Bonn 1, Federal Republic of Germany
[3] Harvard-Smithsonian Center for Astrophysics, 60 Garden St., Cambridge, MA 02138, USA
[4] Haystack Observatory/NEROC, Westford, MA 01886, USA
[5] National Radio Astronomy Observatory, Edgemont Road, Charlottesville, VA 22901, USA
[6] Onsala Space Observatory, S-43900 Onsala, Sweden
[7] Cornell University, Ithaca, NY 14853, USA
[8] NASA, Goddard Space Flight Center, Code 693, Greenbelt, MD 20771, USA
[9] Jet Propulsion Laboratory, 4800 Oak Grove Drive, Pasadena, CA 91109, USA

Received March 19, accepted May 29, 1984

Summary. We observed the quasars 1038+528 A and B with VLBI at λ 2.8, λ 3.6, λ 13 and λ 18 cm at various times between November 1979 and March 1981. The compact radio structure of the A quasar ($z=0.678$) is of the "core-jet" morphological type with a jet whose brightness temperature is only about 1% of that of the core at λ 13 cm and extends beyond 50 mas (~400 pc; $H_0=60$ km s^{-1} Mpc^{-1}, $q_0=0$) from the core with the same orientation ($PA\sim22$ deg) as a radio feature of the core. The jet has a steep spectral index ($\alpha<-0.7$, $S\propto\nu^{\alpha}$) and is not visible at shorter wavelengths, where we see only a core and another feature ~1.7 mas (~13 pc) away from it at $PA\sim17$ deg. We find that the position on the sky of the brightness peak of the core depends on λ, the observing wavelength, and we propose an *ad hoc* law $k\lambda^{\beta}$ with $0.7<\beta<2$ (70% confidence limit) where k is a normalization constant such that the separation of the peaks at λ 3.6 and λ 13 cm is ~0.7 mas (6 pc).

The morphology of the B quasar ($z=2.296$) is also of the "core-jet" type with a very short jet (~6 mas or, equivalently, ~70 pc in extent) and with a spectral index that becomes very steep at the tail, reaching a value $\alpha<-1.9$ between λ 3.6 and λ 13 cm – the steepest spectral index yet reported in extragalactic compact sources.

The B quasar has remained static during the span of time studied, whereas a new component may have emerged from the core of the A quasar. If real its separation rate from the core would be at least 2c. By contrast, we find that the cores of the quasars are stationary with respect to one another, to within the uncertainty of about 0.02 mas/yr (70% confidence).

Key words: VLBI – mapping – astrometry – radiosources – quasars

1. Introduction

The radio sources 1038+528 A and B, about 33″ apart on the sky, were discovered by Owen *et al.* (1978). Optical identification and spectra show the A and B sources to be quasars with $m_v\sim17.5$ and ~18.5 and $z\simeq0.678$ and ≃2.296, respectively (Owen *et al.*, 1980).

We have undertaken a study of this pair of quasars, primarily with VLBI techniques, in the time and wavelength domains. Because both quasars were observed simultaneously with every telescope participating in the VLBI observations, instrumental and atmospheric effects will be very similar for both quasars. This situation can be used to great advantage in the relative calibration of the quasar maps, in the determination of the spatial position of one quasar with respect to the other, in the development of spectral-index maps for the quasars, and in the estimate of the relative proper motion of the two quasars. We report in this article the results obtained from observations through March 1981. Marcaide and Shapiro (1983) (MS1, hereafter) and Marcaide and Shapiro (1984) (MS2, hereafter) have presented related results. This article is organized as follows: We present a description of our observations and our calibration of the data in Sect. 2. Sections 3 and 4 give a detailed account of the mapping and astrometric techniques we have used. In Sect. 5 we discuss the results for the two quasars and for the determination of the relative positions; we also make a few comments on 1038+528 A as a gravitational lens. Finally, in Sect. 6, we present our conclusions.

2. Observations

The VLBI observations were made with the Mark III system. For each session we used a subarray of the following radio telescopes (with the abbreviation subsequently used, the antenna diameter, and the antenna location given in parentheses): DSS14/Goldstone (*D*, 64 m, California); DSS63/Robledo (*M*, 64 m, Spain); Effelsberg (*B*, 100 m, Federal Republic of Germany); Fort Davis (*F*, 26 m, Texas); Green Bank (*G*, 43 m, West Virginia); Haystack (*K*, 37 m, Massachusetts); Onsala (*S*, 25 m and *X*, 20 m, Sweden); Owens Valley (*O*, 40 m, California). We present a summary of the observations in Table 1.

The data from all observations in Table 1 were recorded with a bandwidth of 28 MHz, except for OBS4 for which a 56 MHz bandwidth was used; in all cases correlation was carried out with the Mark III processor (Rogers *et al.*, 1983) at the Haystack

Send offprint requests to: J.M. Marcaide[2]

Table 1. Summary of VLBI observations reported in this article.

Observations	Date	Subarray[a]	Wavelength	Polarization[b]	Duration
OBS1	1979 Nov 23–24	*BGKXO*	3.6 cm	RCP	8 hr[c]
OBS2	1980 May 24–25	*(B)(F)GKO*	2.8	LCP	12
OBS3	1980 Jul 25–26	*BFKSO*	13	RCP	8
OBS4	1980 Dec 6	*FGKO*	2.8	LCP	12
OBS5	1981 Feb 6–7	*(B)F(G)KSO*	18	LCP	12
OBS6[d]	1981 Mar 17–18	*DMBGKO*	3.6	RCP	12
OBS7	1981 Mar 17–18	*DMBGKSO*	13	RCP	12

[a] The station symbols are as defined in the text. The parentheses indicate that the stations did not operate satisfactorily. For details, see Marcaide (1982).
[b] RCP and LCP mean right-circular and left-circular polarization, respectively.
[c] The end of the first three hours are separated from the start of the last five by exactly 24 hr due to constraints of the experiment which was primarily designed by the Goddard-Haystack-MIT group to test the MkIII system.
[d] OBS6 and OBS7 took place simultaneously.

Observatory in Westford, MA. Of all the observations, OBS6 and OBS7 were by far the most successful in the sense that all the scheduled telescopes performed very well, except for a technical difficulty at station *D* which caused half of the observations at that station to be lost. The other experiments were plagued by various problems; for a detailed account, see Marcaide (1982).

The amplitude data were calibrated initially by applying to the correlation coefficients the following calibration factor:

$$\left(\frac{T_{s_{1,j}}}{\Sigma_1 g_{1,j}}\frac{T_{s_{2,j}}}{\Sigma_2 g_{2,i}}\right)^{1/2}$$

where, for a given station i and datum j, $T_{s_{i,j}}$ is the system temperature, Σ_i the sensitivity in Kelvins per Jansky, and $g_{i,j}$ the normalized telescope gain. The T_s were always measured during the experiments. The Σ and g were estimated from available information: published results, measurements by contemporaneous observers, and measurements we made on calibrator sources during the experiments. Consistency checks were made when possible by comparing correlated fringe amplitudes from different baselines at neighbouring uv-points. The reliable estimation of Σ and g was not always possible for OBS1 through OBS5, and especially for OBS2 and OBS4 at the G station. Our use of the data, explained below, diminished the relevance of this missing information. For OBS6, which, with OBS7, forms the backbone of this article, calibration was set by the M station, where precise measurements of T_s were made and where Σ was both well known (Turegano, private communication) and similar to that at the D station (Turegano and Klein, 1980). Our calibration of the B station provided the standard for OBS7.

The absolute flux density calibration is estimated to be accurate to within 10% whereas the relative calibration for data from a given baseline is probably reliable to within 4%. Typical telescope performance is shown in Table 2.

3. Mapping

Having calibrated the visibility amplitude data in this manner, we used the Caltech Mapping Package, kindly made available to us by T. Pearson, to make preliminary hybrid maps of the quasars A and B independently. Final adjustment to the radiometry and to these hybrid maps was made using the CORTEL algorithm (Cornwell and Wilkinson, 1981) in a version called AMPHI, kindly provided by S. Unwin. Our data provided a stringent test of AMPHI because both sources were observed simultaneously (the telescopes were all pointed towards a position midway between the two sources and the smallest telescope beam was about twice the source separation) and because the visibility amplitude data for both sources were subjected to the same initial calibration. Thus, except for the effects of mispointing of the telescopes, the corrections for each antenna found by AMPHI should be the same for both sources. Indeed they were, as shown in Table 3. We used the average of each of these correction factors as our final correction factor for the data for both A and B to obtain the final hybrid maps from OBS6 and OBS7 presented in Figs. 1a and 1b for the A quasar and in Figs. 2a and 2b for the B quasar. We also made hybrid maps with AIPS (Fomalont, 1982), which uses the adaptive calibration

Table 2. System temperatures, T_{sys}, estimated for the points of highest antenna sensitivity in Jansky equivalent for each of the antennas participating in the observations made on 1981 March 17–18. The scale is estimated to be correct to within 10% and the relative values to within 4%. Antenna symbols are as defined in the text

Station	T_{sys}(Jy)	
	3.6 cm	13 cm
K	1000	4046
G	1073	435
B	146	78
O	1052	508
D	54	25
M	43	31
S	-	773

Table 3. Antenna-based visibility amplitude correction factors deduced using AMPHI (see text) for the A and B quasars at λ 3.6 and λ 13 cm. The factors are rounded. The symbol *F* indicates the value actually used for both quasars in constructing hybrid maps. Antenna symbols are as defined in the text.

		K	*G*	*B*	*O*	*D*	*M*	*S*
λ 3.6 cm:	*A*	1.00	0.99	1.015	1.01	1.00	0.98	–
	B	0.995	0.98	1.005	1.01	1.01	0.99	–
	F	1.00	0.985	1.01	1.01	1.005	0.985	–
λ 13 cm:	*A*	1.01	1.01	0.98	1.02	1.02	0.96	1.00
	B	1.02	1.02	0.98	1.02	1.02	0.95	1.01
	F	1.015	1.015	0.98	1.02	1.02	0.955	1.005

scheme proposed by Schwab (1980). The maps obtained with AIPS were almost identical to those presented in Figs. 1 and 2, with minor differences in detail at the level of the lowest contour shown. The comparisons of the predictions from these maps with the corresponding data are shown in Figs. 3a and 3b for the A quasar and Figs. 4a and 4b for the B quasar.

In Fig. 5 we present the same model as in Fig. 1b, but convolved with a CLEAN beam about one order of magnitude larger to correspond to use of data only from the "short" baseline interferometers that are sensitive to the extended emission. We discuss this map and the others in Sect. 5.

It has been recognized (see, for example, Wilkinson, 1983) that systematic errors in the calibration limit the dynamic range of hybrid maps, preventing the noise limit from being reached. All our maps are limited by systematic errors in spite of our best calibration effort. We estimate the noise in the map of the A quasar in Fig. 1a to be approximately 4 mJy/beam, based on the approach of estimating the lowest believable brightness temperature contour and the flux density per beam in the strongest feature in the map. This map noise is about 20–30 times higher than the computed thermal noise. The map of the B quasar in Fig. 2a has lowest believable contours comparable to those of the map in Fig. 1a, but the peak brightness of the B quasar is about five times lower than that of A. We therefore estimate that the noise in the map in Fig. 2a is about 0.75 mJy/beam. (We confirm this estimate with an independent method described in Sect. 5.2.) This map noise is about five times higher than the computed thermal noise. Thus, for sufficiently weak sources (i.e. peak brightness $\lesssim$ 20 mJy/beam), the thermal noise may be the factor limiting the dynamic range of the maps.

By choosing a reference point in the hybrid map for the A quasar as a phase reference, we made a map of the B quasar for each of the wavelengths of observation using the technique described in MS2. The phase-reference maps were not of higher dynamic range than those presented in Figs. 1b and 2b. Since the dynamic range of all the maps is set by the defective amplitude calibration instead of by thermal noise, the recovery of the degrees of freedom by use of a phase reference, which should lower slightly the thermal noise in the map made from data from a seven antenna array, is nearly irrelevant.

A major advantage of using the phase reference technique is that it determines the relative positions of the two sources on

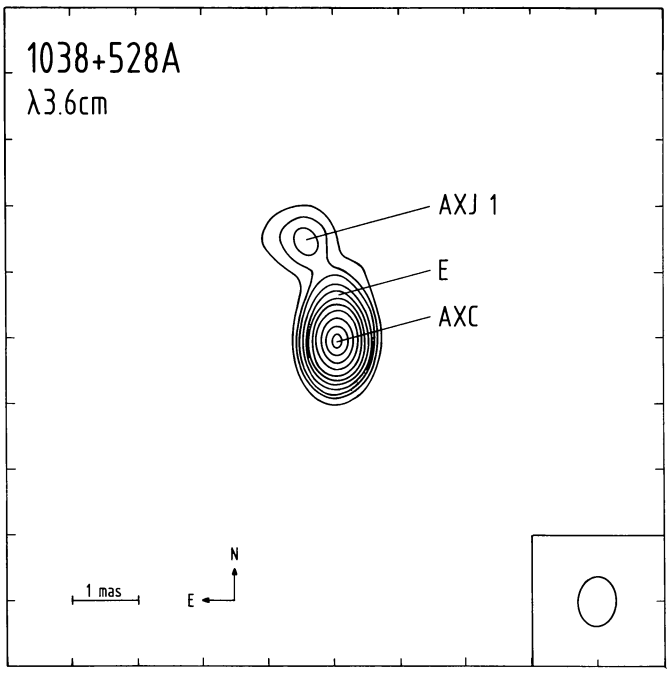

a

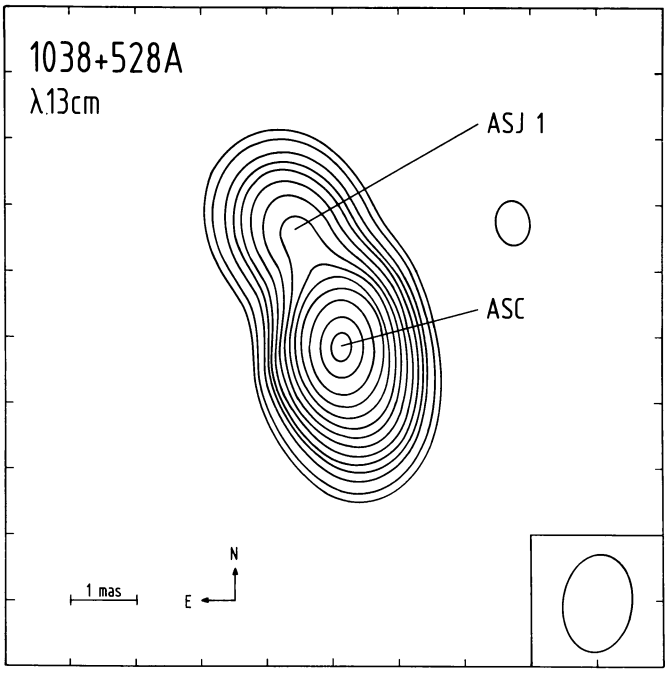

b

Fig. 1. a Hybrid map of the A quasar obtained from the 1981 March 17–18 observations at λ 3.6 cm. Boxed in the lower-right-hand corner is the CLEAN beam used to restore the map. The total flux density in the map is 440±45 mJy and the peak brightness temperature is ~1.4 10^{10} K. The contours specified are −1, 2, 4, 6, 10, 15, 22, 30, 42, 60, 80 and 95% of the peak brightness temperature. There are no negative contours down to the specified value. The map components are labelled (see text). **b** Same as **a**, but at λ 13 cm. The total flux density in the map is 320±32 mJy and the peak brightness temperature is ~2.3 10^{10} K. (Note that the restoring beam we have used for λ 13 cm is only twice that of the beam used in **a** for λ 3.6 cm. Had we used a beam four times instead of twice larger the peak brightness temperature would have been four times lower.) The contours specified are −1, 2, 3, 5, 7, 9, 12, 16, 21, 27, 35, 45, 60, 80 and 95% of the peak brightness temperature. There are no negative contours down to the specified value

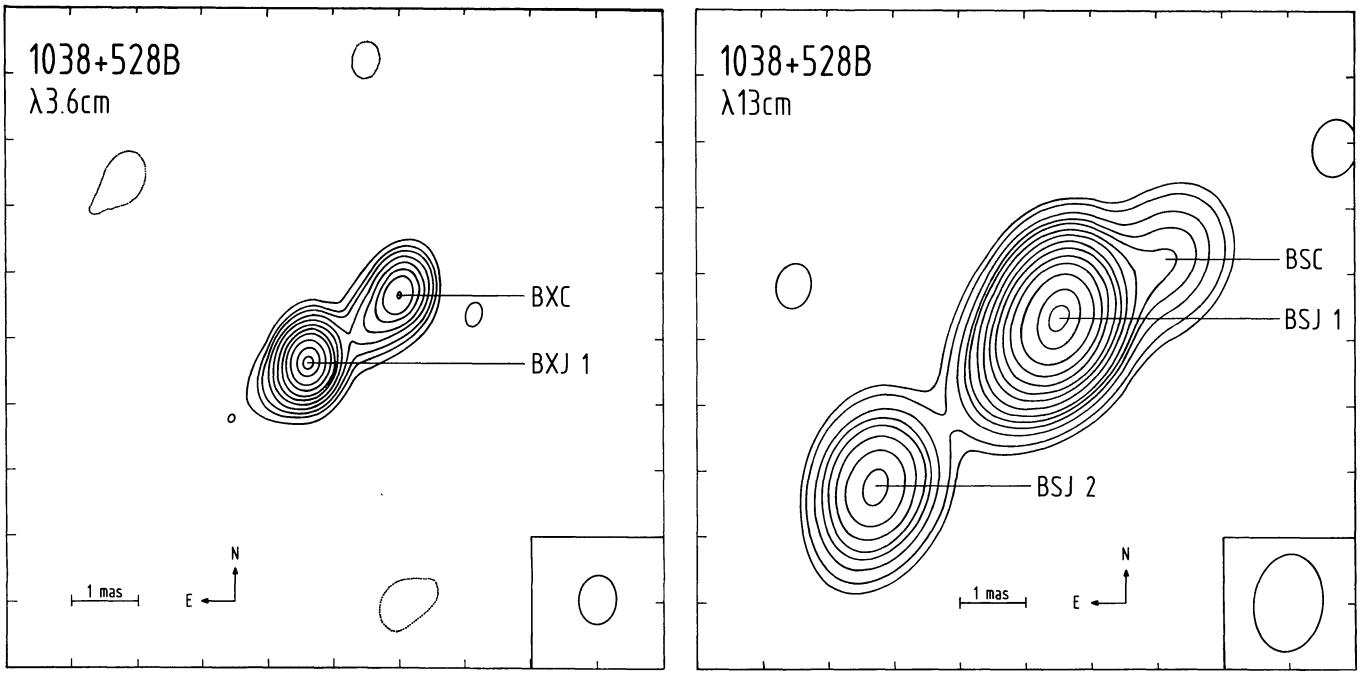

Fig. 2. a Same as Fig. 1a, but for the B quasar. Total flux density in the map is now $\sim 88 \pm 9$ mJy. The peak brightness temperature is $\sim 2.1\ 10^9$ K. The negative contours are plotted as dashed lines. **b** Same as Fig. 1b, but for the B quasar. The total flux density in the map is 125 ± 13 mJy and the peak brightness temperature $\sim 1.1\ 10^{10}$ K

the sky, thus providing a constraint on maps made at several epochs and wavelengths. These constraints are especially stringent if one source is point-like (see Bartel et al., 1984), or if the structure of the reference and object source – often approximately one-dimensional in brightness – are mutually perpendicular, the latter being approximately our case. Figure 1 of MS2 shows the relative positions of the quasars A and B in OBS6 and OBS7 and a suggested registration of the two sets of maps.

For experiments OBS1 through OBS5, the paucity of data prevented our mapping the B quasar. Even the A quasar, typically three or five times stronger than the B quasar and hence detectable with more interferometers, could not be mapped from data from OBS3 and OBS5. We used AMPHI with the λ 3.6 cm map from the 1981 March 17–18 data as an initial model, for mapping the A quasar from the data from OBS1; the resulting map is presented in Fig. 6a. Here the map was "restored" from the CLEAN components with the circular beam shown boxed in the same figure. The restoration of the maps by circular beams shown in Figs. 6a for OBS1 and 6b for OBS6 (actually the same result as shown in Fig. 1a, but restored with a different beam), was made to show more clearly the possible existence of an extension towards the north of the main feature in the map of Fig. 6b which is not clearly visible in Fig. 6a. In Fig. 7 we compare the data for the A quasar from OBS1 with the predictions from the maps shown in Figs. 6a and 6b. In Fig. 8, we present the corresponding comparison between the results obtained from OBS6 (see Fig. 2a and Fig. 4a) and the data for the B quasar obtained from OBS1. Clearly the map from OBS6 gives a good representation of the data of the B quasar at the time of experiment OBS1, approximately 17 months earlier.

Our treatment of the data from OBS2 and OBS4 was identical with nearly identical results: having calibrated as best we could the limited visibility amplitude data from each experiment, we mapped the A quasar with AMPHI, using as the initial model the extrapolation to λ 2.8 cm of the map at λ 3.6 cm shown in Fig. 1a. (This extrapolation and the one to λ 18 cm from the map at λ 13 cm (see Sect. 5.3.) were made using the estimates of the spectral indices of the source components as presented by Marcaide (1982), p. 110. The missing or excess flux densities were added to or subtracted from the strongest CLEAN component of the source component.) For OBS4 the resulting map and a comparison of its predictions with the data are shown in Figs. 9 and 10, respectively. The corresponding comparison for the B quasar is shown in Fig. 11 (the map itself is not presented because it is the extrapolation to λ 2.8 cm of the map at λ 3.6 cm shown in Fig. 2a).

For OBS3 we did not attempt mapping since the maps from OBS7, shown in Figs. 1b and 2b, provided predictions that represented adequately the poor data from OBS3. The few and poorly calibrated data from OBS5 were ignored since they were taken close in time and wavelength to OBS7. We used only the phase information from the interferometer with the longest baseline for differential astrometry (see Sect. 5.3.)

4. Differential astrometry

We determined the relative positions of the A and B quasars for OBS1 through OBS7 with the technique described in MS1. That is, we determined at each wavelength the relative positions of two reference points, one each chosen in the map of each of the two quasars. We chose as reference the location of the brightest CLEAN component in the map. For some experiments, we did not obtain maps but instead relied on the results from OBS6 and

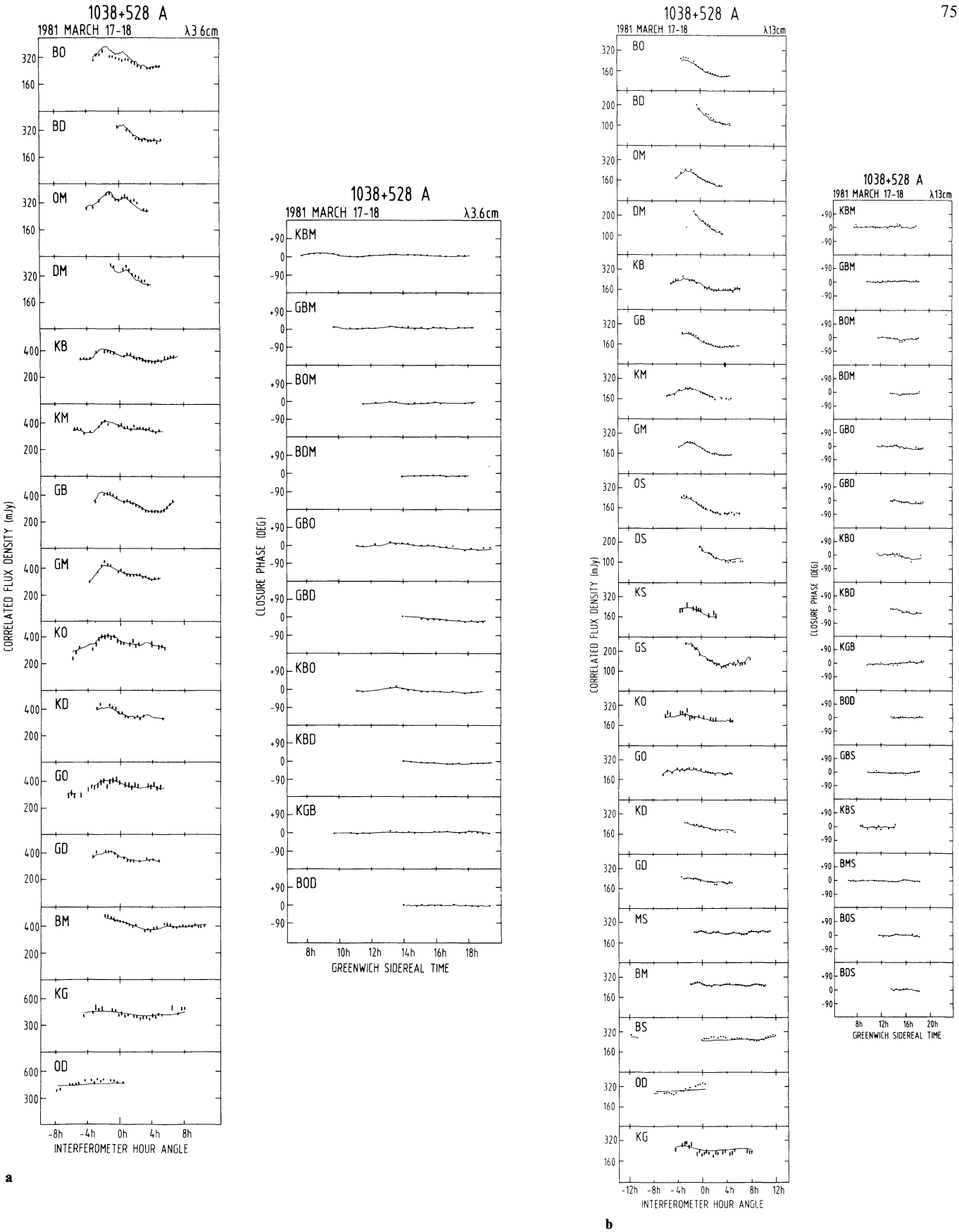

Fig. 3. a Predictions from the A quasar map shown in Fig. 1a (solid line) compared with the observed visibility amplitudes and closure phases. The symbols of the interferometers and triplets of stations are as throughout the text. The display has been arranged to show the interferometers approximately in order from those with longest to those with shortest baselines. Thus, the results from physically similar interferometers can be readily compared. An arrangement that allows a similar comparison has been made for the closure-phase display. Only independent closure phases are presented. **b** Same as **a**, but for map shown in Fig. 1b

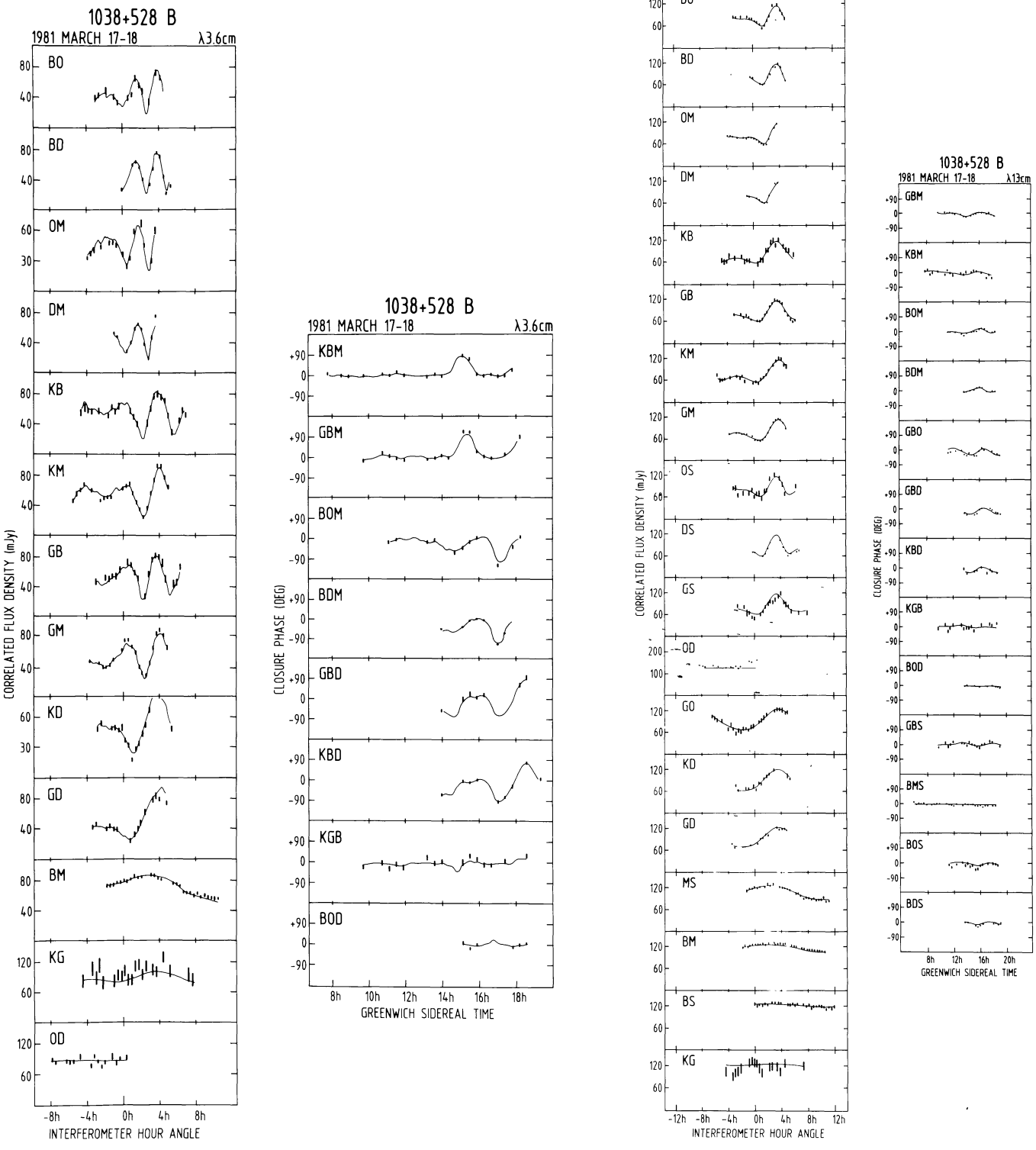

a **b**

Fig. 4. a Same as Fig. 3a, but for B quasar and for map shown in Fig. 2a. **b** Same as Fig. 3a, but for B quasar and for map shown in Fig. 2b

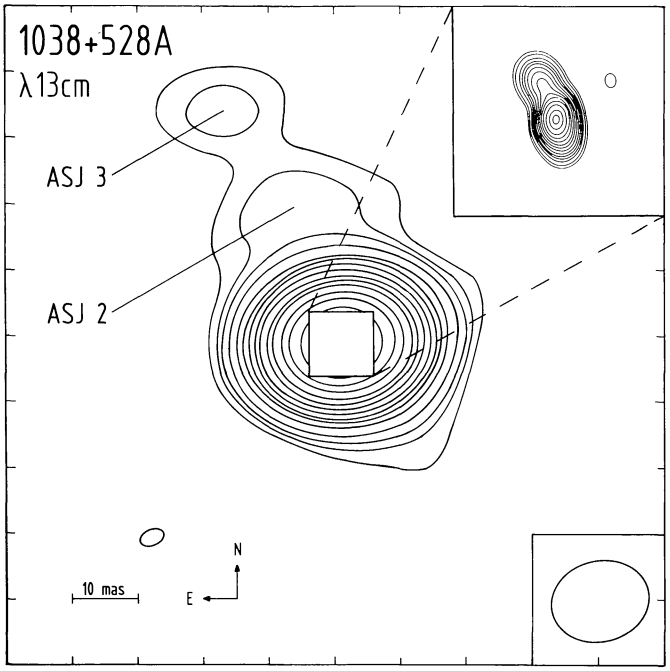

Fig. 5. Same map as in Fig. 1b, but with a CLEAN restoring beam about ten times larger. This restoring beam is the half power gaussian adjustment to the main lobe of the "dirty" beam for observations with only the short baseline interferometers in the array: KG, BS, BM, MS, and OD. The map in Fig. 1b is inset in the upper side corner of this figure with the broken lines indicating the relative scales

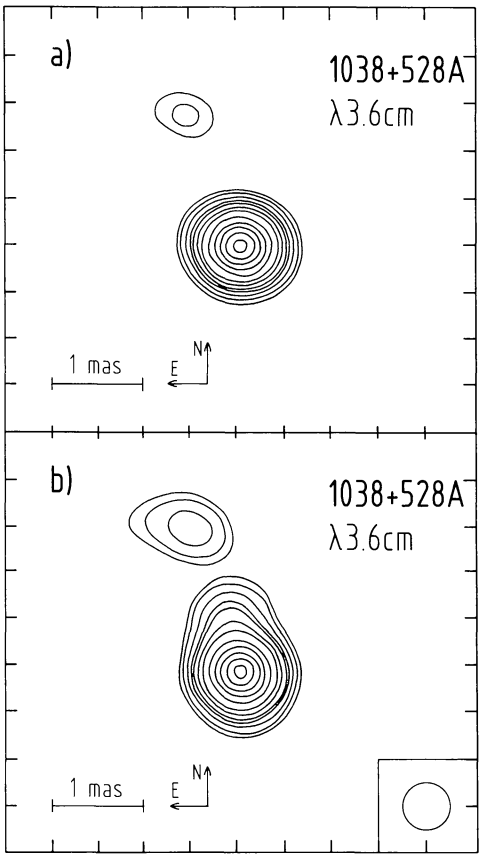

Fig. 6. a and b. Hybrid maps of the A quasar at λ 3.6 cm made from the **a** 1979 November 25–26 and **b** 1981 March 17–18 data. The map in **b** is the same as that in Fig. 1a, but here a circular restoring beam shown in the box has been used; see text

OBS7 in the way explained in Sect. 3. All the astrometric results are summarized in Table 4 and presented in Fig. 12. Results obtained from reliance on information external to the experiment itself have been indicated in Table 4 with an asterisk and a short explanation, and in Fig. 12 with dotted error bars.

The astrometric technique, which uses phase information (see MS1), is to a large degree complementary to the phase-reference mapping technique (see MS2). Both techniques determine the relative positions of the maps of the two quasars and the results of the application of each technique can be used profitably with the other technique. For phase-reference mapping a certain minimum amount of data is necessary; for differential astrometry the corresponding minimum amount is much less; further, most of the information is contained in the data from the interferometers with the longest baselines, provided there is available a reasonable *a priori* map for the sources. The astrometric technique will check how well such maps fit the phase-delay data: poor maps will produce, in general, large, systematic postfit phase-delay residuals. Of course, it is conceivable that even a poor map could yield acceptably small postfit residuals, especially if *few* phase-delay data are available. Another difference is one of resolution: whereas the maps have milliarcsecond resolution, the differential astrometric technique may produce one or two orders of magnitude more precise determinations of the relative positions. The risks of interpretation of the astrometric results which may arise because of this resolution mismatch are discussed in MS1. Nevertheless, it was not stressed there that true systematic changes in the structures (or in the sky positions of the reference points) might be seen with the astrometric technique before they are apparent in the maps.

We do not show here any postfit residuals (one example was shown by MS1), but we note that χ^2 per degree of freedom typically ranged between two and three, where the measurement standard errors reflected solely the signal-to-noise ratios. Numerically, for our most accurate data, the rms of the postfit residuals was under 2 ps, equivalent to 0.6 mm in light travel distance.

5. Discussion

The overall flat spectrum of the system 1038+528 A, B shown in Fig. 13 seems to be a coincidental balancing of the spectra of the individual A and B quasars. Between λ 3.6 and λ 13 cm, their spectra have indices $\alpha = 0.2 \pm 0.2$ ($S \propto \nu^{\alpha}$) and $\alpha = -0.30 \pm 0.25$, respectively. The index for A is consistent with the λ 3 mm total flux density measurement, indicating a very short wavelength turnover for some feature in the A quasar, likely its core, which has $\alpha = 0.4 \pm 0.2$ between λ 3.6 and λ 13 cm, and which is probably an X-ray emitter (Owen et al., 1981).

Below we discuss first the morphology and then the spectral indices of each of the quasars independently. For this discussion, features in the maps in Figs. 1 and 2 of each of the quasars have been labelled with the following symbols: A or B for A or B quasar, respectively, X or S for λ 3.6 or λ 13 cm, respectively, C for core and J for jet. A number n following the symbol J will denote the nth feature in the jet, with the other $(n-1)$

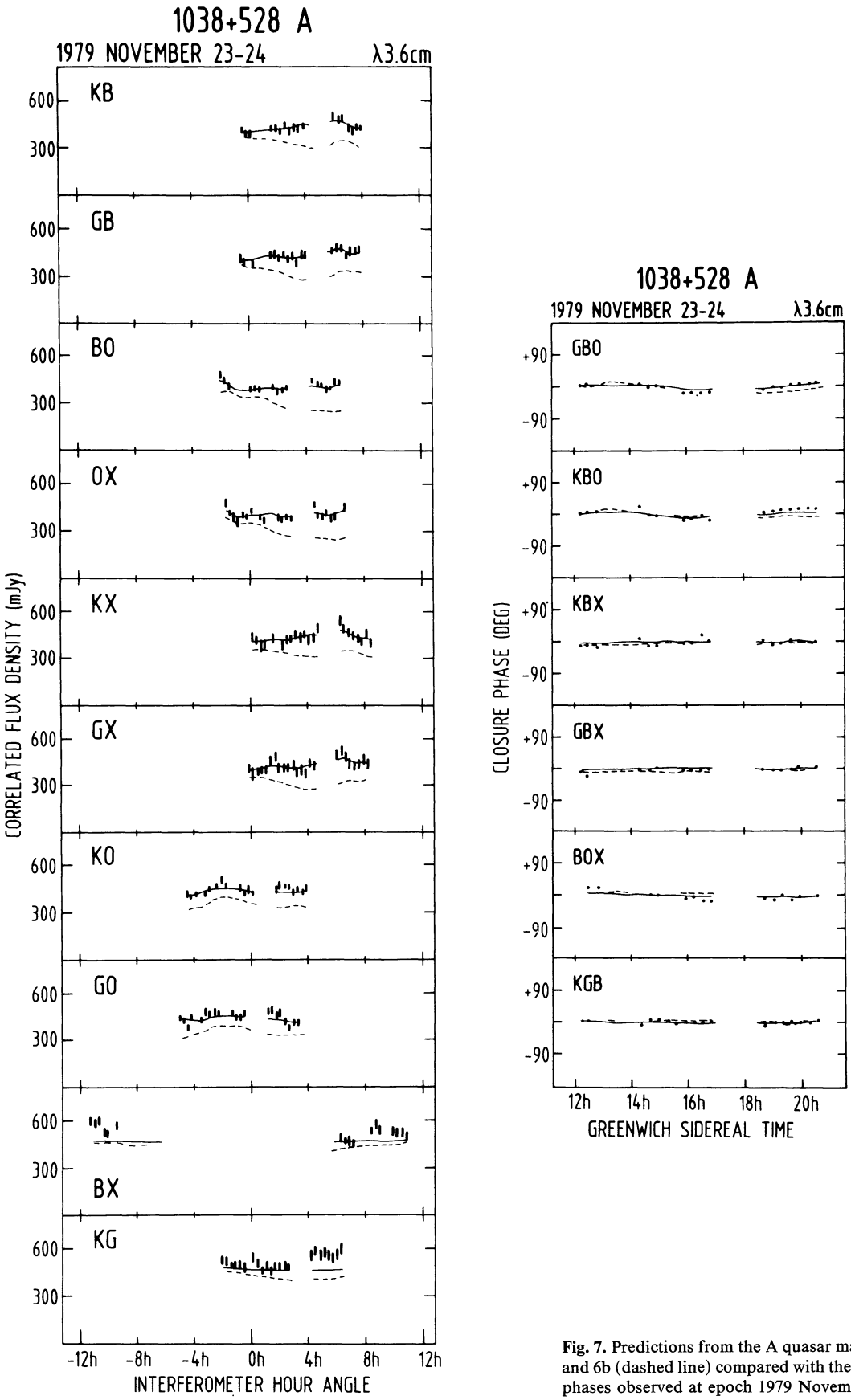

Fig. 7. Predictions from the A quasar maps shown in Figs. 6a (solid line) and 6b (dashed line) compared with the visibility amplitudes and closure phases observed at epoch 1979 November 25–26

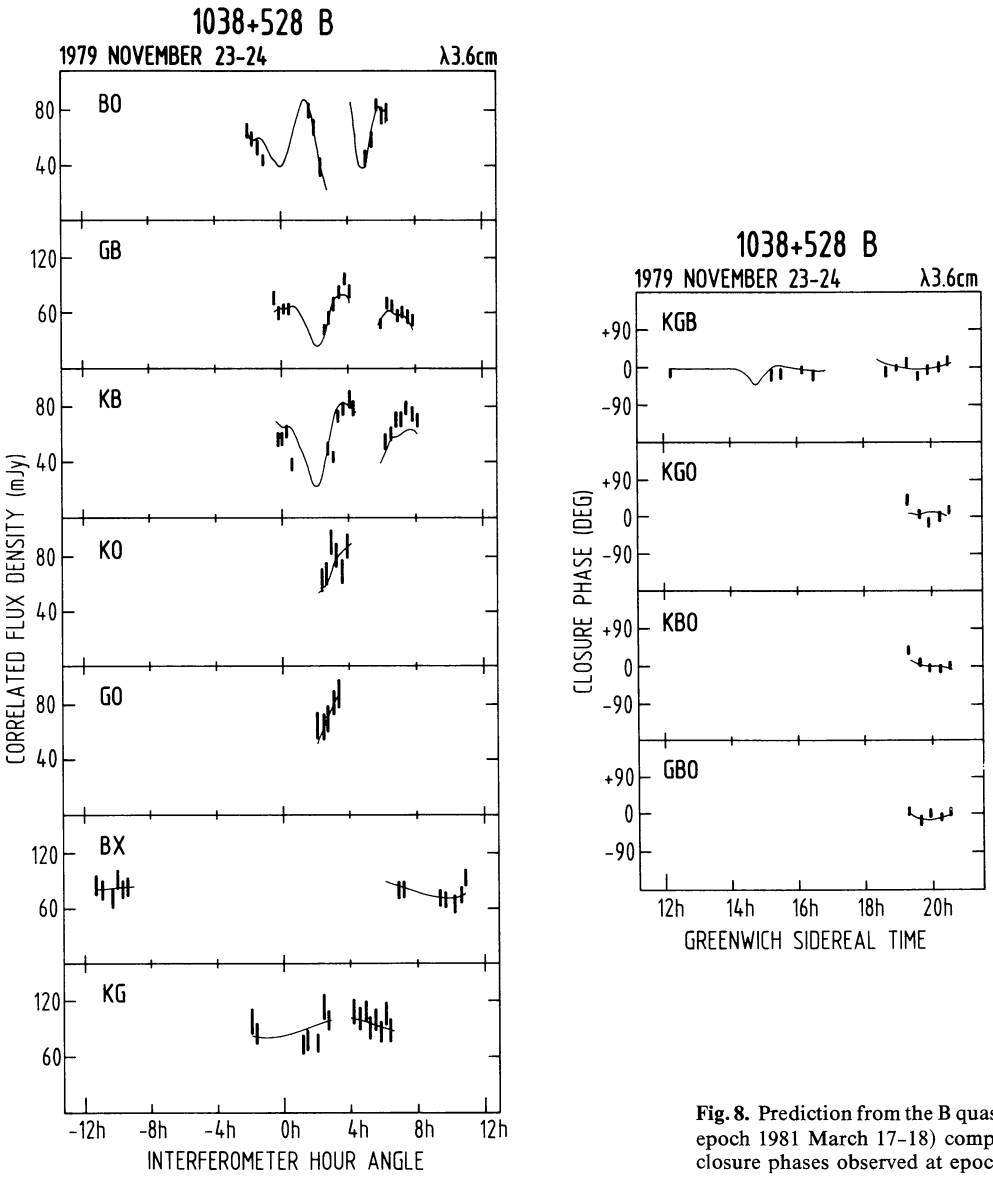

Fig. 8. Prediction from the B quasar map shown in Fig. 2a (corresponding epoch 1981 March 17-18) compared with the visibility amplitudes and closure phases observed at epoch 1979 November 25-26

features in the jet being closer to the core. For example, BSJ2 will describe the second closest feature to the core in the jet for the B quasar in the λ 13 cm map.

5.1. 1038+528 A

In the map at λ 3.6 cm, Fig. 1a, we can distinguish two features: the stronger, AXC, and the weaker, AXJ1, ~1.7 mas away at a position angle (PA) of ~17 deg. AXC has no discernible elongation towards the south but has a definite elongation towards the north. We denote this extension at PA ~ 0 deg as *E*, departing from the nomenclature since it is not a distinct feature. In the map at λ 13 cm, Fig. 1b, we can distinguish again two dominant features, ASC and ASJ1. ASJ1 is at PA ~ 22 deg, ~1.7 mas away from the peak brightness of ASC. The core feature ASC appears somewhat extended to the southwest, but the extension is not well determined because the resolution obtained from the λ 13 cm array was insufficient for this purpose. In addition, the position of ASJ1 relative to that of ASC is not so well determined as is the corresponding position of AXJ relative to AXC. In the map at λ 13 cm shown in Fig. 5, we can see two additional features in the jet: ASJ2 and ASJ3. At least two questions arise: (i) How can we register Figs. 1a and 1b? (ii) Does *E* represent an intrinsic elongation of AXC or is it a new component being ejected from AXC? We address these in turn.

Given that the features AXC and AXJ1 at λ 3.6 cm, and ASC and ASJ1 at λ 13 cm, are in the same relative positions, it would seem natural to superpose them as is commonly done with VLBI maps. This approach is incorrect in our case, as discussed in MS2: Within an uncertainty of ~0.1 mas, only one registration of the two maps of the A and B quasars appears reasonable. With the registration chosen in MS2, neither AXC and ASC nor AXJ1 and ASJ1 are related features. In fact, AXC is not even collinear with ASC and ASJ1 and its position would lie somewhere in the southwest extension of ASC.

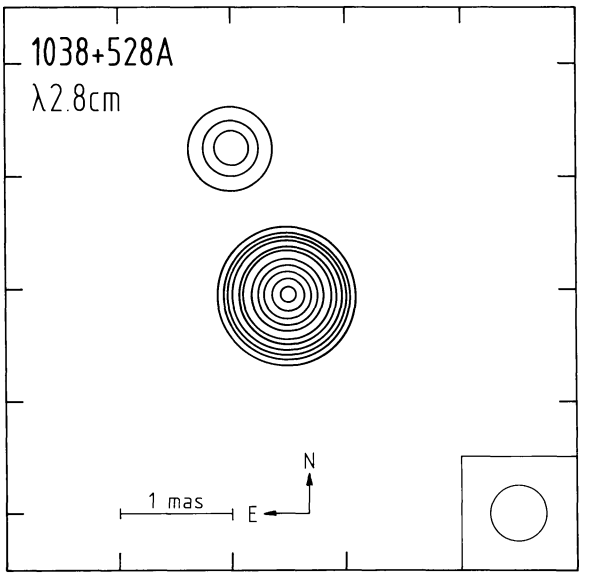

Fig. 9. Hybrid map of the A quasar at λ 2.8 cm from observations at epoch 1980 December 6. The restoring beam used is the same as that used in Fig. 6 to allow comparison. This beam is unrealistically small for the baseline lengths involved

A spectral index map, shown in Fig. 2a of MS2 has the following morphology: a small core region with a strongly inverted spectral index ($\alpha \gg 0$) and a jet along which the spectral index first becomes flat ($\alpha \simeq 0$) and then progressively steeper ($\alpha \ll 0$). The change of the spectral index along the jet (PA$\sim$ 20 deg) is shown in Fig. 14. The decrease of α in the direction opposite to the jet is likely an artifact of the reconstruction method and such a decrease would not exist had we used some "overresolution".

At least three features (ASJ1, ASJ2, and ASJ3) can be seen in the $\sim$400 pc long jet (here and hereafter $H_0 = 60$ km s^{-1} Mpc^{-1}, $q_0 = 0$), suggesting a history of ejections of energetic electrons from the core as manifested by its apparently very short turnover wavelength. In regard to *E*, consider Figs. 6a and 6b. In Fig. 6a from OBS1, an experiment made 17 months before OBS6, we see no evidence of *E*, whereas we see AXJ1 unequivocally since its position relative to that of AXC is the same for both epochs. Furthermore, the strength of AXJ1 is comparable, if not identical, at both epochs. We cannot totally rule out the existence of *E* at the epoch of OBS1 from the available data. If *E* arose as an ejection from AXC sometime in the 17 month interval between OBS1 and OBS6, the transverse component of its ejection velocity exceeded 2*c*. Only three months before OBS6, that is for OBS4 (see Fig. 9), we also find no evidence of *E* whereas again AXC and AXJ1 are present. Here our resolution was much lower than for OBS1 and OBS6, because of the absence of intercontinental baselines, which unfortunately prevents us from saying anything meaningful about the existence of *E* in December 1980.

The ratio of the flux density in the map of the A quasar to that in the map of the B quasar (see below), as well as our total flux density measurements, seem to indicate that the A quasar contained slightly more flux density (50–100 mJy) in OBS1 than in OBS6. Seielstad et al. (1983) have monitored at λ 2.8 cm the flux density of 1038+528 from 1979 through 1983. Our measurements are consistent with theirs for the two epochs of OBS1 and

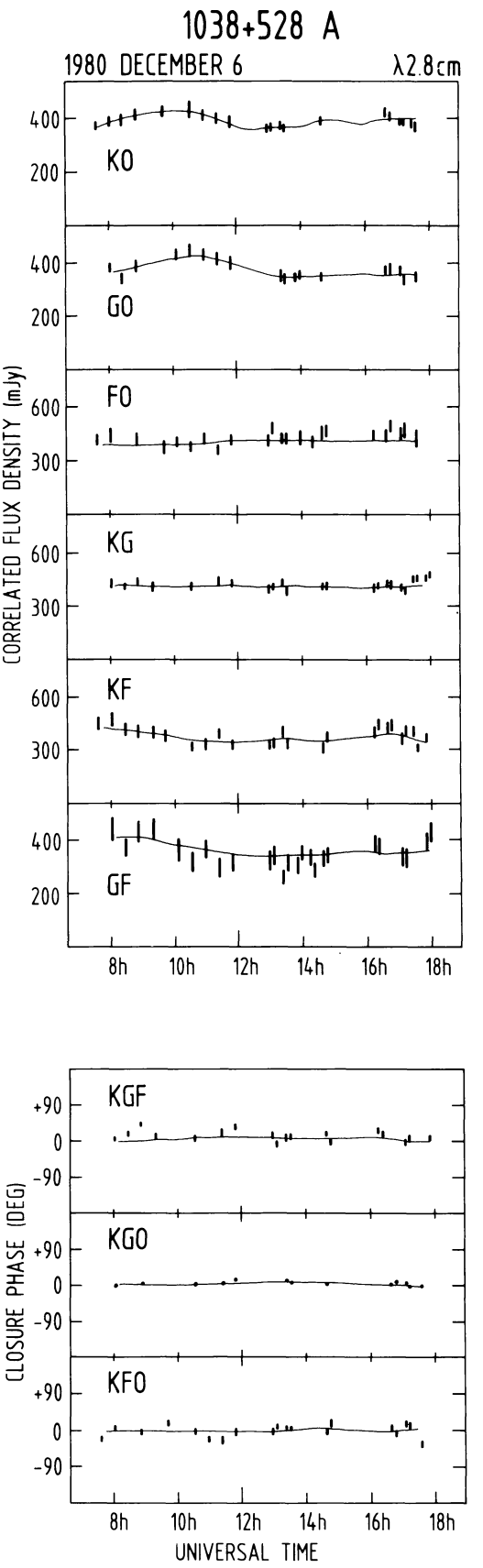

Fig. 10. Comparison of the predictions from the A quasar map shown in Fig. 9 (solid line) with the observed visibility amplitudes and closure phases

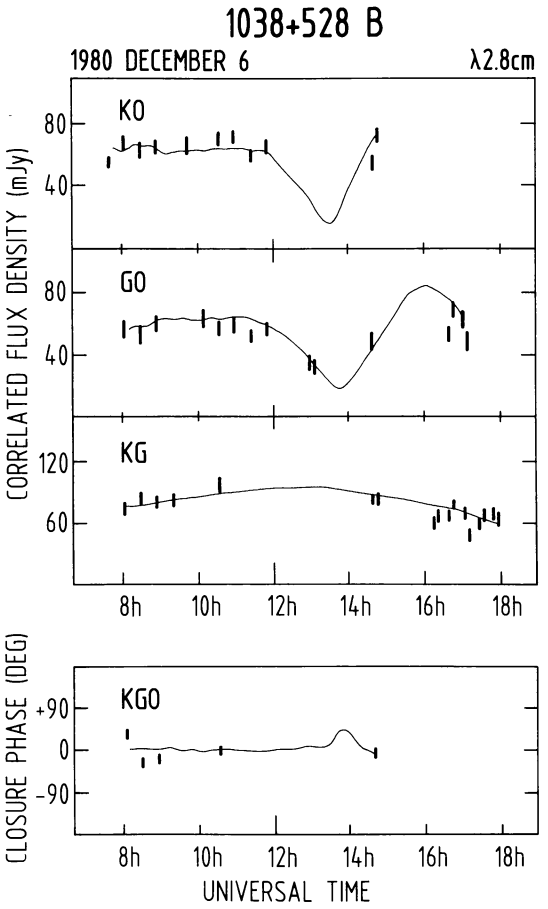

Fig. 11. Comparison of the predictions from the B quasar model at λ 2.8 cm, obtained by extrapolating the map for λ 3.6 cm (see text), with the visibility amplitudes and closure phases observed at epoch 1980 December 6

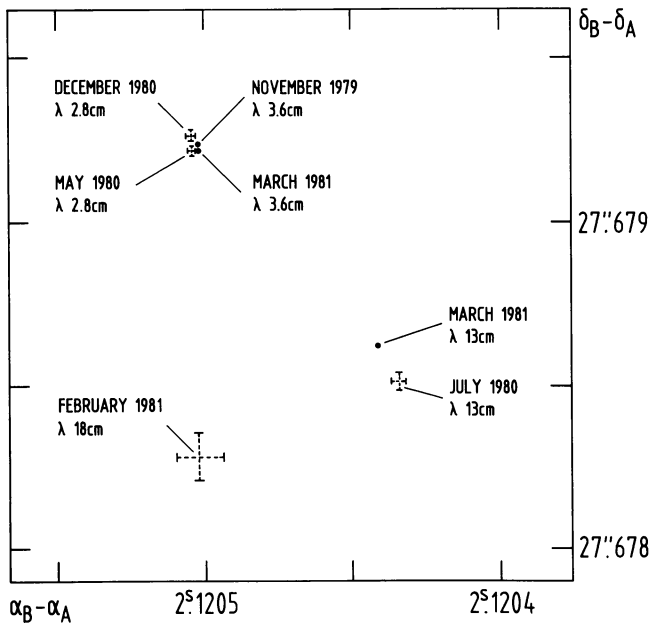

Fig. 12. Positions of the B quasar minus that of the A quasar for all observations (1950.0). See text and Tables 1 and 4

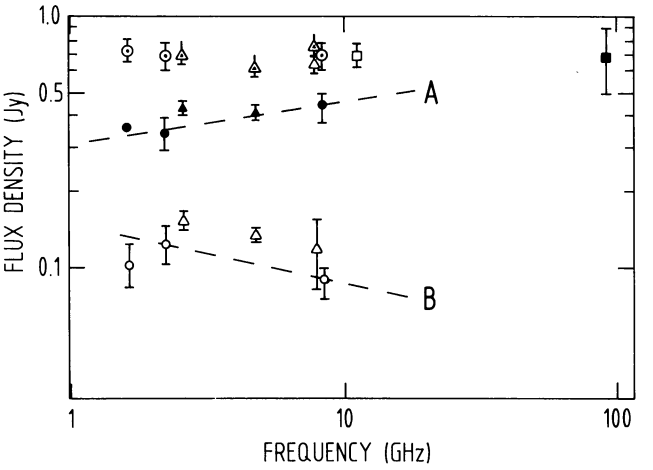

Fig. 13. Radio spectra for 1038+528 A and B. The empty symbols indicate measurements for the B quasar. The same filled symbols indicate measurements for the A quasar. The symbols in the upper part of the graph indicate measurements for the total system 1038+528 which besides the A and B quasars includes weak extended emission straddling the A quasar (see Marcaide, 1982). The dashed lines indicate the spectra for the A and B quasars as estimated from OBS6 and OBS7 (see text). The figure includes all the available data regardless of epoch of observation: circles, Marcaide 1982; triangles, Owen et al. 1978, Owen et al. 1980; empty square, Seielstad et al. 1983; filled square, Cotton (unpublished)

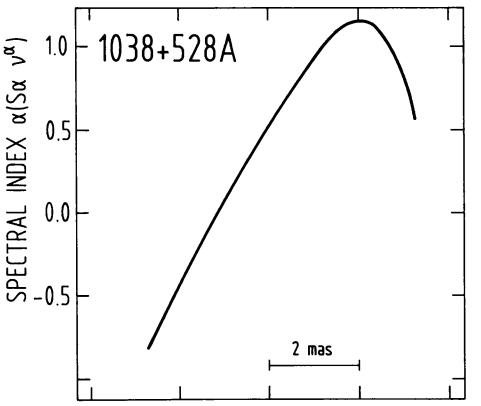

Fig. 14. Profile along PA 20 deg of the spectral-index map shown in Fig. 2a of Marcaide and Shapiro (1984)

OBS6. However, Seielstad et al. seem to measure significant variability in the flux of 1038+528 during 1979. According to our picture of 1038+528 (see below) the core of the A quasar would be responsible for this variability and it is tantalizing to think that the feature *E* in this core may be the new component created in the small outburst of 1979 as seen two years later.

In short, there seems to be evidence of moderate activity in this core-jet radio source as manifested by flux density variations and the emergence of a possible new component from the core. This picture is consistent with the structure found along the jet indicating past activity. The core has a pronounced inverted spectrum and substantial emission even at a wavelength of 3 mm. The spatial location of the peak of emission of the core depends on the wavelength of observation, probably indicating optical depth variations with wavelength.

Table 4. Positions of the B quasar minus that of the A quasar, found using the technique described by Marcaide and Shapiro (1983). The sky position (1950.0) used for the A quasar was ($\alpha = 10^h38^m43^s.132$, $\delta = 52°49'10''.35$)

Wavelength	Epoch	RA[a] (1950.0)	DEC[a] (1950.0)
2.8 cm	1980.4	$2^s.1205030 \pm 0^s.0000010$	$27''.679229 \pm 0''.000015$[b]
2.8	1980.9	2.1205028 ± 0.0000012	27.679270 ± 0.000017[b]
3.6	1979.9	2.1205005 ± 0.0000007	27.679246 ± 0.000005[c]
3.6	1981.2	2.1205009 ± 0.0000002	27.679228 ± 0.000003
13	1980.6	2.120434 ± 0.000002	27.67850 ± 0.00003[d]
13	1981.2	2.1204408 ± 0.0000006	27.678622 ± 0.000009
18	1981.1	2.120502 ± 0.000008	27.67829 ± 0.00007[e]

[a] The uncertainty shown is the formal standard error, determined by scaling the measurement standard deviations uniformly such that the root-weighted-mean-square of the postfit residuals is unity.
[b] Extrapolated map of the B quasar used for removing the structure contribution to the differenced phase-delay observable (see Marcaide and Shapiro, 1983). The extrapolation was made from the map of the B quasar from epoch 1981.2 on the basis of the spectrum of the individual map components deduced from Figs. 1 and 2.
[c] Map of the B quasar from epoch 1981.2 used for removing the structure contribution to the differenced phase-delay observable.
[d] Same as (c) but for the maps of the A and B quasars.
[e] Same as (b) but for the maps of the A and B quasars.

5.2. 1038+528 B

The λ 3.6 cm map in Fig. 2a shows two features separated by ~1.7 mas at PA ~ 127 deg. The southeast feature, denoted BXJ1, is stronger than the northwest one, BXC. In the λ 13 cm map in Fig. 2b we see a feature, denoted BSJ2, ~4 mas southeast (PA ~ 133 deg) of an elongated feature. This elongated feature in Fig. 2b is barely split into two features of which the southeast feature is much stronger. The PA of the line joining these two features is therefore not so well determined as are the other two position angles given above. The separation of the features and the position angle of this line (~1.7 mas and ~125 deg, respectively) are approximately the same as those for BXJ1 and BXC. This relationship (confirmed by MS2 from phase-reference maps) prompts us to denote these components as BSJ1 and BSC.

We conclude that quasar B is a "core-jet" source, with the core, BXC or BSC, at the northwest end. At the opposite end of the short jet is the component BSJ2 whose spectral index is so steep that it is invisible in our λ 3.6 cm map. The position angle of the line joining the jet feature BXJ1 (or BSJ1) to the core is 5 ± 2 deg different from the position angle of the line joining the jet feature BSJ2 to the core, thus suggesting that the "core-jet" structure suffers a slight bend. The registration, discussed in MS2, of the A and B quasars implies a particular spectral-index map shown in Fig. 2b of MS2. The profile of that map along the direction of the jet (PA ~ 133 deg) is presented in Fig. 15. In order to estimate a bound on the spectral index at BSJ2 we selected a "window" that included a large part of BSJ2 on the λ 13 cm map, but no significant flux density on the λ 3.6 cm map, both of these maps having been reconstructed using a restoring beam (FWHM) corresponding to the λ 13 cm data (i.e. beam of $0''.0030 \times 0''.0022$ with major axis at PA −15 deg). We estimated the total flux density in this window for both maps. For the λ 3.6 cm case, we were estimating only the contribution of noise, i.e. an upper bound on the flux density of the feature, not present in this map. From the window area of about 4.4 mas^2, we obtained about 0.6 and 9.0 mJy from the λ 3.6 and λ 13 cm maps, respectively. Thus, $\alpha_{BJ2} < -2$. Increasing the size of the window just enough to pick up in one corner emission on the λ 3.6 cm map yields 1.0 and 14.0 mJy for the contributions from λ 3.6 and λ 13 cm, respectively, and the same limit $\alpha_{BJ2} < -2$. Considering that the flux density scale at each wavelength is in error by at most 10%, we obtain $\alpha_{BJ2} < -1.9$, the steepest spectral index yet reported in the compact (mas) structures of quasars.

The effective arrays used in OBS1 through OBS5 were insufficiently sensitive to allow us to map the B quasar since its total flux density is only 88 ± 8 and 125 ± 13 mJy at λ 3.6 cm and λ 13 cm, respectively. Nevertheless, these experiments showed that there were no significant departures from the structure deduced from the 1981 March 17–18 experiment, as mentioned

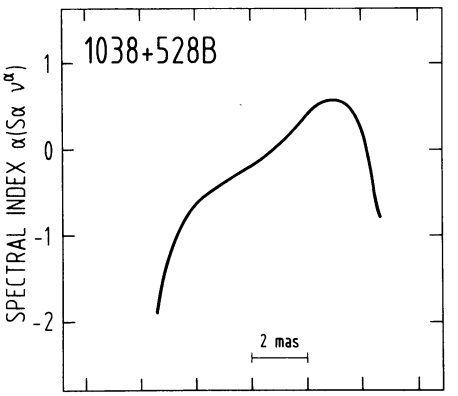

Fig. 15. Profile along PA 133 deg of the spectral-index map shown in Fig. 2b of Marcaide and Shapiro (1984)

in Sect. 3 and shown by Fig. 8. This conclusion is consistent with the astrometric results which probe the phase information (see Fig. 12).

5.3. Relative Positions

To determine the relative positions of the A and B quasars, we chose as the reference position in each the CLEAN component of maximum flux density which is near the point of peak brightness intensity (of course, if convenient at some later epoch, a different reference can be selected and the data re-analyzed). The separation, if any, between the position of this CLEAN component and that of maximum flux density depends on the steepness of the peak and on the resolution available in the experiment. For our maps, these separations are very small except for the map of A at λ 13 cm, where it may be as much as $\sim$0.1 mas. The reference point in the A quasar is close to the peak of the emission from the core, whereas, for the B quasar, the reference point is close to the peak of the emission from a feature in the jet. The relative positions on the sky of the reference points in the A and B quasars, obtained from all four of our λ 2.8 cm and λ 3.6 cm experiments, lie within 0.065 mas (70% confidence) of each other. If we consider only the λ 3.6 cm data, the separations are within 0.025 mas (70% confidence) which is equivalent to a bound of $\sim$0.018 mas/yr on the proper motion of the two references.

The difference of $\sim$0.7 mas between the relative positions of A and B obtained from the analysis of the λ 3.6 and λ 13 cm observations (Fig. 12) is statistically very significant. We believe that this difference is due to an intrinsic wavelength dependence of the position of the peak of the brightness intensity in the core of the A quasar (see also MS2). Although it is conceivable that the core is clumpy and that the component "labelled" core at λ 3.6 cm is totally self-absorbed at λ 13 cm, this assumption would not alone explain why the peak for the λ 13 cm map does not have a counterpart in the λ 3.6 cm map. For this explanation to be valid, a λ 6 cm map of the A quasar would have to have a very unusual elongated core with a poorly defined peak. This does not seem to be the case (M. Reid, private communication, 1982). High dynamic range maps at λ 6 cm of the A quasar, referenced to the B quasar, however, are essential to answer the question definitively. (We recently made successful λ 6 cm observations; these are now in the early stage of reduction.)

The position of the peak brightness of the core may represent the point at which a smooth jet becomes optically thin (see, for example, Blandford and Königl, 1979). In this case, the peak would appear at different sky positions at different wavelengths. We have attempted to formulate a wavelength dependence law, $k\lambda^{\beta}$ (k a normalization constant) for the position of this peak with respect to the (hypothetical) position for $\lambda = 0$. With the data plotted in Fig. 12, we can restrict the range of β to $0.7 < \beta < 2$ (70% confidence). If the "smooth-jet" hypothesis is correct, the result from the λ 6 cm experiment should allow the range of β to be reduced by a factor of about three.

We also considered the possibility that a nonuniform cloud of ionized gas along the line of sight to the quasars might be responsible for this difference in position of the peaks. This hypothesis can be discarded, even without resort to detailed calculations, because the signature of the dependence of the relative positions of the peaks on wavelength would then follow a λ^2 law, whereas comparisons of the results from OBS5 and OBS7 with those form OBS6 and OBS7 are inconsistent with this hypothesis. Indeed in Fig. 12 the difference in the relative positions of the quasars at λ 3.6 cm and λ 18 cm is about the same (at PA$\sim$35 deg) as at λ 3.6 and λ 13 cm, instead of twice as large, as a λ^2 law would demand. [The difference in the relative positions obtained from the data at λ 13 cm and λ 18 cm along PA$\sim$133 deg may be caused by an imperfection in our extrapolation of the structure from λ 13 to λ 18 cm (i.e. by using $\alpha_{BJ2} = -1.5$ instead of, say, $\alpha_{BJ2} = -1.9$). Due to practical problems we have been unable to investigate this point thoroughly.]

5.4. Comments on 1038+528 A as a gravitational lens

The detection of gravitational lens systems, especially 0957+561 (see, for example, Walsh et al., 1979), prompted us to consider 1038+528 as such a system in which the A quasar is the lens. The image of the B quasar we see would be a distortion of the "true" B quasar and a second image of it (let us call it B′) would be to the southwest of the A quasar. A detection of B′ would provide a confirmation of this scenario as well as an estimate of the mass of the A quasar. Simple computations show that for "reasonable" point-like quasar masses ($\sim 10^{13}\, M_{\odot}$) the flux density of B′ would be three orders of magnitude below the detection limit of our VLBI experiment ($\sim$1 mJy); detection with a somewhat more sensitive instrument like the VLA is also infeasible and, in addition, would be hampered by the lack of resolution of that instrument since B′ would probably be closer than 0.″1 to the A quasar. Naturally these conclusions would be wrong were the mass of the A quasar to be unexpectedly large (10^4 to $10^{15}\, M_{\odot}$) or were a large group of galaxies to be near the A quasar. Nonetheless, we have not yet attempted a systematic search for B′.

Dyer and Roeder (1982), who considered these ideas independently, established an upper bound for the mass of the A quasar with a method that depended crucially on : (i) the estimation of the axial ratio of the dominant (and assumed elliptic) feature in the observed B quasar; and (ii) the assumption that the axial ratio of this feature for the "true" B quasar is unity. Even if the feature chosen were the quasar core the latter assumption may well be incorrect. Moreover, the VLBI feature assumed by these authors to be the core is not the core. The lack of detection of component BSJ2 in the experiment whose results they used, together with their lack of spectral information, prompted their incorrect interpretation of the VLBI structure. It is not clear to us how the method of Dyer and Roeder should be applied to the structures shown in Figs. 2a and 2b, at λ 3.6 and λ 13 cm, respectively, because, for example, at λ 3.6 cm the core, BXC, is somewhat elongated, but the only visible jet features at this wavelength, BXJ1, looks spherically symmetric. Considering that parsec-sized structures of quasars are often one-dimensional, with features, especially those in the jet, somewhat elongated along the structure axis of the source and seldom perpendicular to it, we find that the gravitational lens distortion should be minimal for the feature BXJ1. Hence the mass of the A quasar probably much lower than the mass limit given by Dyer and Roeder. In making this statement, we are ignoring the lensing effect of any possible group of galaxies at the redshift of the A quasar.

6. Conclusions

The A and B quasars have "core-jet" morphologies. Without the observations at λ 13 cm, made with the most sensitive VLBI array

ever used, we might have concluded wrongly, from shorter wavelength observations alone, that both sources were "doubles". The core of the A quasar dominates its morphology at centimetric wavelengths with the brightness temperature of its ~400 pc long jet being about one hundredth that of the core. By contrast, the "jet" in the B quasar is very short (~70 pc) since its spectral index undergoes a dramatic steepening from 0.7 to less than −1.9. The tail of this jet has the steepest spectral index found to date in extragalactic compact sources, indicating high electron energy losses as being responsible for the shortness of the jet. We find over a span of two years no evidence for appreciable morphological changes in the B quasar, whereas a new feature may be emerging from the A quasar core at superluminal speed.

In a related paper (MS2), use of the phase-reference mapping technique suggests that the correct registration of the λ 3.6 cm and λ 13 cm maps of both quasars is constrained to lie within ~0.1 mas from the one proposed. With this registration, two main results were found: (i) The peaks of brightness in the core of the A quasar at λ 3.6 and λ 13 cm are separated on the sky by ~6 pc; and (ii) Both quasars present a very similar spectral-index morphology in spite of their different radio morphology.

Determination of the relative position of the A and B quasars from use of astrometric techniques at four different wavelengths supports an *ad hoc* law, $k\lambda^{\beta}$ (k, a normalization constant) for the wavelength dependence of the position of the peak brightness in the core of the *A* quasar relative to the hypothetical position at $\lambda = 0$. This range is $0.7 < \beta < 2$ (70% confidence). The likely narrowing of this range from the results of an experiment at λ 6 cm should allow a useful prediction to be made of the position of the peak at λ 1.3 cm which could be checked by VLBI.

Acknowledgements. We thank everyone who made possible these early Mark III observations, and very especially John Ball, the Haystack Observatory staff, and the Deep Space Network staff for their important help with the March 1981 observations. J.M.M.'s research at the Max-Planck-Institut für Radioastronomie was supported in part by the NASA-JPL Contract 956542. Research at the Massachusetts Institute of Technology and the Harvard-Smithsonian Center for Astrophysics was supported in part by the National Science Foundation, Grant AST-8022229. Research at the Jet Propulsion Laboratory was supported in part by the NASA Contract 7-918.

References

Bartel, N., Ratner, M.I., Shapiro, I.I., Herring, T.A., Corey, B.E.: 1984, Proceedings of IAU *Symp.* No. 110 eds. Fanti, R., Kellermann, K.I., and Setti, G., Reidel, Dordrecht, 113

Blandford, R.D., Königl, A.: 1979, *Astrophys. J.* **232**, 34

Cornwell, T.J., Wilkinson, P.N.: 1981, *Monthly Notices Roy. Astron. Soc.* **196**, 1067

Dyer, C.C., Roeder, R.C.: 1982, *Astrophys. J.* **256**, 386

Fomalont, E.B.: 1982, in *Image Display Processing and Analysis in Synthesis Mapping*, Proceedings of the NRAO-VLA Workshop, Socorro, N.M., June 1982. eds. Thompson, A.R., and D'Addario, L.R. (National Radio Astronomy Observatory)

Marcaide, J.M.: 1982, Ph.D. thesis, Massachusetts Institute of Technology

Marcaide, J.M., Shapiro, I.I.: 1983, *Astron. J.* **88**, 1133

Marcaide, J.M., Shapiro, I.I.: 1984, *Astrophys. J.* **276**, 56

Owen, F.N., Porcas, R.W., Neff, S.G.: 1978, *Astron. J.* **83**, 1009

Owen, F.N., Wills, B.J., Wills, D.: 1980, *Astrophys. J. Letters* **235**, L57

Owen, F.N., Helfand, D.T., Spangler, S.R.: 1981, *Astrophys. J. Letters* **250**, L55

Rogers, A.E.E., Cappallo, R.J., Hinteregger, H.F., Levine, J.I., Nesman, E.F., Webber, J.C., Whitney, A.R., Clark, T.A., Ma, C., Ryan, J., Corey, B.E., Counselman, C.C., Herring, T.A., Shapiro, I.I., Knight, C.A., Shaffer, D.B., Vandenberg, N.R., Lacasse, R., Mauzy, R., Rayhrer, B., Schupler, B.R., Pigg, J.C.: 1983, *Science* **219**, 51

Schwab, F.R.: 1980, Proceedings SPIE **231**, 18. 1980 International Optical Computing Conference

Seielstad, G.A., Pearson, T.J., Readhead, A.C.S.: 1983, *Publ. Astron. Soc. Pacific* **95**, 842

Turegano, J.A., Klein, M.J.: 1980, *Astron. Astrophys.* **86**, 46

Walsh, D., Carswell, R.F., Weymann, R.J.: 1979, *Nature* **279**, 381

Wilkinson, P.N.: 1983, in *VLBI Techniques*, Proceedings of the Toulouse Meeting - August 1982 (Cepadues Editions)